OPEN ACCESS
IOP Publishing
Nanotechnology

Nanotechnology **35** (2024) 395709 (8pp)
https://doi.org/10.1088/1361-6528/ad5e87

Valence-state mixing and reduced magnetic moment in $Fe_{3-\delta}GeTe_2$ single crystals with varying Fe content probed by x-ray spectroscopy

D Backes[1,*], R Fujita[2], L S I Veiga[1], D A Mayoh[3], G D A Wood[3], S S Dhesi[1], G Balakrishnan[3], G van der Laan[1] and T Hesjedal[2]

[1] Diamond Light Source, Harwell Science and Innovation Campus, Didcot OX11 0DE, United Kingdom
[2] Department of Physics, Clarendon Laboratory, University of Oxford, Oxford OX1 3PU, United Kingdom
[3] Department of Physics, University of Warwick, Coventry CV4 7AL, United Kingdom

E-mail: dirk.backes@diamond.ac.uk

Received 14 March 2024, revised 9 June 2024
Accepted for publication 3 July 2024
Published 15 July 2024

Abstract

We present a spectroscopic study of the magnetic properties of $Fe_{3-\delta}GeTe_2$ single crystals with varying Fe content, achieved by tuning the stoichiometry of the crystals. We carried out x-ray absorption spectroscopy and analyzed the x-ray circular magnetic dichroism spectra using the sum rules, to determine the orbital and spin magnetic moments of the materials. We find a clear reduction of the spin and orbital magnetic moment with increasing Fe deficiency. Magnetic susceptibility measurements show that the reduction in magnetization is accompanied by a reduced Curie temperature. Multiplet calculations reveal that the Fe^{2+} state increasingly mixes with a higher valence state when the Fe deficiency is increased. This effect is correlated with the weakening of the magnetic moment. As single crystals are the base material for exfoliation processes, our results are relevant for the assembly of 2D magnetic heterostructures.

Supplementary material for this article is available online

Keywords: xmcd, Fe3GeTe2, sum rules analysis, multiplet calculations, x-ray absorption spectroscopy

1. Introduction

The emergence of graphene [1] in 2004 was the starting point for a series of discoveries of 2D materials with novel electronic and topological properties, also giving rise to the question whether there are 2D magnets, and if so, what kind of magnetic order to expect. Despite theoretical predictions that ferromagnetism is not possible in monolayers [2] (in the absence of magnetic anisotropies), magnetically ordered 2D materials, such as CrI_3 [3] and $Cr_2Ge_2Te_6$ [4] were discovered, albeit with low ordering temperatures. This motivated an intense search for 2D magnets with higher transition temperatures. A promising candidate is Fe_3GeTe_2, exhibiting 2D ferromagnetism with strong perpendicular anisotropy [5] and a transition temperature of around 225 K [6–9].

Many follow-up experiments have examined the magnetic [5, 10–23] and transport properties [24–28] of Fe_3GeTe_2

* Author to whom any correspondence should be addressed.

and their manipulation. Indeed, in gate-tunable monolayers of Fe_3GeTe_2, room temperature ferromagnetism has been demonstrated [28]. Furthermore, due to the breaking of inversion symmetry at interfaces and surfaces, the Dzyaloshinskii–Moriya interaction (DMI) [29] can give rise to the formation of skyrmions [30–35].

Structurally, Fe_3GeTe_2 belongs to the $P6_3/mmc$ space group, where a layer of Fe_3Ge is sandwiched between two layers of Te. The Fe atoms occupy two non-equivalent sites with Wyckoff positions of 4e for the Fe I site and 2c for the Fe II site. The Fe I atoms can be found in a hexagonally ordered layer with C_{3v} site symmetry, while the Fe II atoms form covalent bonds with Ge in another, adjacent layer and exhibit D_{3h} site symmetry [6, 36]. The Fe_3Ge layers are separated by van der Waals gaps above and below which the Te layers reside. The existence of van der Waals gaps, across which the bond strength is reduced, allows for the convenient exfoliation of 2D layers from single crystals.

A well-known problem is that the magnetic properties of such van der Waals magnets can show large variations. These variations occur between flakes exfoliated from different single crystals but also when exfoliated from different parts of the same single crystal [37]. Furthermore, their small lateral size of only a few tens of micrometers reduces the number of applicable characterization techniques. Spectro-imaging techniques, such as x-ray photoemission electron microscopy, are limited in accessibility and the measurement process is very time-consuming. Hence, establishing a pre-characterization method for the base materials, i.e., the Fe_3GeTe_2 crystals, that can help to optimize the materials parameters and improve their homogeneity is desirable.

The quality and homogeneity of the single crystals is known to be strongly influenced by the growth method [38]. Their stoichiometry is the most important parameter determining the electronic and magnetic properties of these Fe-based compounds [10, 39]. Interestingly, theoretical calculations predict that the ground state of stoichiometric Fe_3GeTe_2 is antiferromagnetically ordered [39], but that the Fe deficiency induces ferromagnetic order. While chemical vapor transport (CVT) leads to single crystals with a uniform composition, crystals grown with the flux method show a large variability of the compositional parameters [38].

In this work, we investigate Fe_3GeTe_2 single crystals produced with varying Fe stoichiometry and its influence on the magnetic properties. We carry out a sum rules analysis of x-ray magnetic circular dichroism (XMCD) spectra to obtain both spin and orbital contributions to the magnetization. The spectra are compared to those obtained from multiplet calculations and a sum rules analysis of the calculated spectra is performed. Magnetic susceptibility measurements shed light on the magnetic transition temperature. We compare the results obtained on samples with different Fe content.

2. Experimental methods

2.1. Crystal growth

$Fe_{3-\delta}GeTe_2$ bulk crystals were grown using both CVT and the flux method using excess Te [38] with δ indicating the Fe deficiency. The compositions of the samples, and thus the values of δ, were obtained by energy-dispersive x-ray (EDX) analysis covering an area of about 500 μm in both lateral directions as reported in [38]. EDX is not an efficient method to determine exact stoichiometries but provides a good indication of relative ratios of the elements in a whole batch of crystals. It is thus extremely useful to establish trends in the composition of a set of samples, as is the case here. We compared $Fe_{3-\delta}GeTe_2$ single crystals grown by CVT and by the flux method. We have chosen three different crystals each with a different Fe stoichiometry for our investigations: one single crystal grown by the CVT technique with stoichiometry of $Fe_{2.84}GeTe_{2.04}$ ($\delta = 0.16$) and two other single crystals grown by the flux method with stoichiometries of $Fe_{2.59}GeTe_{2.08}$ and $Fe_{2.78}GeTe_{2.13}$, i.e., $\delta = 0.41$ and 0.22, respectively. The dimensions of the unit cell were determined to be a = 4.0129(1) Å and c = 16.3428(4) Å, with no discernible differences between crystals grown by the CVT method and those grown by the flux method [38].

2.2. Measurements

X-ray absorption spectroscopy (XAS) measurements were performed at Diamond Light Source on beamline I06. A superconducting vector magnet was used to apply fields of up to 6 T in the direction of the incident x-rays to eliminate magnetic domains. The XMCD was obtained by subtracting XAS spectra obtained with right (pc) and left circular polarized (nc) light with respect to the k vector, using total electron yield (TEY) detection mode. The bulk crystals were cleaved immediately before the measurements in the sample preparation chamber of the magnet at a base pressure of 10^{-7} mbar. All measurements were taken at a temperature of 2 K and a base pressure of 10^{-10} mbar. Hence, the exposure to oxygen is greatly reduced, but oxidation can never be completely excluded. For this reason, a separate study has been carried out that shows that oxygen is not the origin of the second Fe-L_3 peak (see figure S1 in the Supplemental Materials [40]). Energy scans were taken over a range of 695 to 738 eV to capture the Fe $L_{2,3}$ edges. The beam size of ≈200 μm horizontally and ≈100 μm vertically is much smaller than the area probed by EDX. Hence, the composition can be regarded as homogeneous within the probed area.

The magnetic properties of the single crystals were measured using a Quantum Design Magnetic Property Measurement System (MPMS) superconducting quantum interference device (SQUID) magnetometer. The measurements were made in the temperature range between

2 and 300 K in various applied magnetic fields using the field-cooling (FC) protocol. In contrast to the surface sensitive TEY measurements using x-rays, a SQUID probes the whole bulk of the crystal. Hence, a small amount of surface oxidation due to exposure to air will not be visible, and cleaving of the crystals is not required.

All samples used were flat platelets and could easily be mounted on sample holders for x-ray spectroscopy and SQUID measurements, minimising any error in aligning with respect to the x-rays or magnetic fields.

3. Results and discussion

3.1. X-ray absorption spectroscopy

The orbital and spin moments of Fe sites were determined from XAS and XMCD spectra [41–43]. In figure 1(a), the XAS spectra of the sample with $\delta = 0.41$ taken with pc and nc polarization are shown as an example. The spectra were first normalized by the slope of the pre-edge background of the L_3 peak, then subtracted from one another and subsequently normalized by the post-edge background of the L_2 peak. For the quantitative analysis, the continuum-state background was removed using a smooth step function with a ratio of 2:1 between the L_3 and L_2 steps. The XMCD in figure 1(b) was obtained by subtracting the pc from the nc spectra. The right-hand side scale represents the integrated XMCD, from which the quantities $p = -\int_{L_3}(I_{pc} - I_{nc})$ and $q = -\int_{L_3,L_2}(I_{pc} - I_{nc})$ are determined (as indicated by the blue arrows). From the integration of the sum of the pc and nc XAS (see figure 1(c), scale on the right-hand side), the quantity $r = \int_{L_3,L_2}(I_{pc} + I_{nc})$ was obtained (see green arrow). The offsets of the integrated XAS and XMCD spectra r, p, and q (see figures 1(b) and (c)) were measured at well-defined energies and kept constant for all samples and spectra. The step function is shown as dashed line in figure 1(c).

The orbital m_{orb} and spin moments m_{spin} were then calculated using

$$m_{orb} = -\langle L_z \rangle = -\frac{4q}{3r} n_h \quad (1)$$

and

$$m_{spin,eff} = -2\langle S_z \rangle - 7\langle T_z \rangle = -\frac{6p - 4q}{r} n_h \quad (2)$$

with n_h the number of holes in the 3d shell, which is 4 for an Fe atom with 6 electrons in the 3d shell and a valence of 2+ [11]. A value of $n_h = 4$ is correct for ionic bonding, but not for metallic/covalent bonding expected for Fe with a valence of 2+. Hence, n_h is likely to be different from 4, scaling the magnetic moments slightly [44]. Furthermore, we neglect here the presence of higher valence states and will discuss this possibility further below in connection with multiplet calculations. The measured moment $m_{spin,eff} = m_{spin} - 7\langle T_z \rangle$ includes both the spin moment and the magnetic dipole term $\langle T_z \rangle$. The latter is assumed to be zero, or at least small, in case of the half-filled d^5 configuration of Fe^{3+} for the calculation of the spin moment so that $m_{spin,eff} \approx m_{spin}$ [44]. In case of the d^6 configuration in Fe^{2+} it can lead to an error of 10% in the effective spin moment [45].

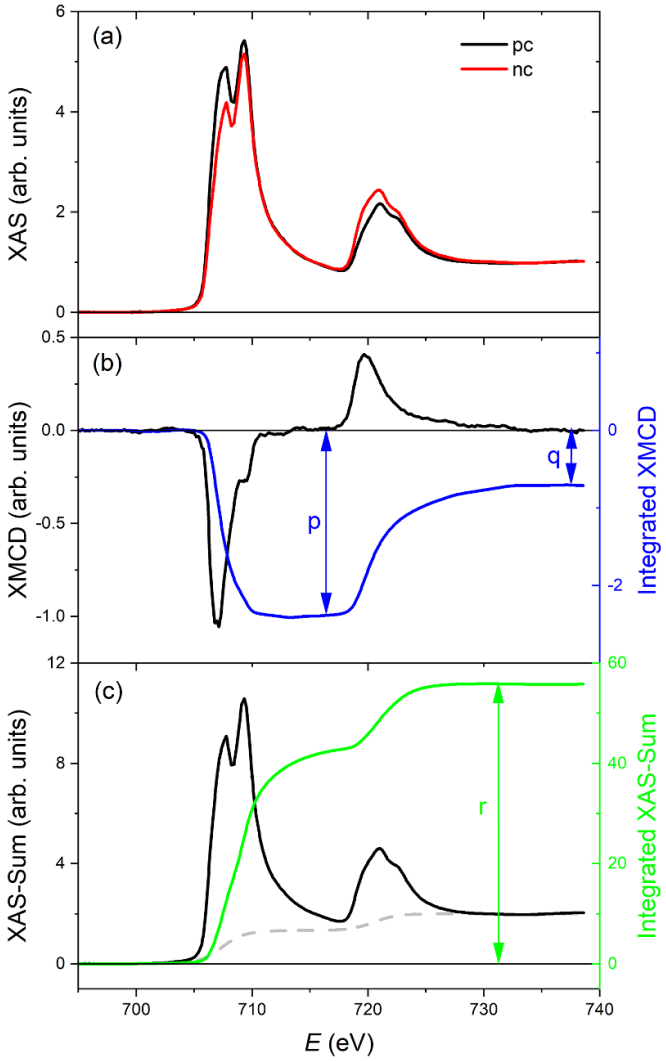

Figure 1. (a) XAS spectra measured with positive (pc, black line) and negative (nc, red line) circular polarization. The data of the sample with $\delta = 0.41$ are shown as an example. (b) Resulting XMCD spectra (black line) and integrated XMCD (blue line) from which the quantities p and q are obtained. (c) Sum of pc and nc XAS (black line) and the integrated XAS-Sum (green line), from which the quantity r is obtained. A smooth step function is used to represent the continuum-state background (gray dashed line), which is subtracted. A magnetic field of 6 T was applied in the direction of the incident x-rays, perpendicular to the sample surface. The sample temperature was 2 K.

A summary of the results of the sum rules analysis is shown in table 1. The $2p_{1/2}$ - $2p_{3/2}$ intermixing can lead to an error of 10 % in the spin moment, but the orbital moment remains unaffected. The orbital component of the magnetization m_{orb} shows a decrease, within the error bars, from 0.15 to 0.08 μ_B/Fe with increasing Fe deficiency δ. Literature values are either within this range [11, 16] or slightly below [15]. Even clearer is the decrease of the spin moment m_{spin}, falling from 1.26 to 0.84 μ_B/Fe with increasing Fe deficiency. The value reported in [15] is within this range but higher values have been observed

Table 1. Results of the sum rules analysis for all three Fe deficiencies, δ. The magnetic moments m_{spin} and m_{orb} are given in units of μ_B/Fe atom. The number of holes was assumed to be $n_h = 4$.

δ	m_{spin}	m_{orb}	m_{orb}/m_{spin}
0.16	1.26(12)	0.15(2)	0.12(2)
0.22	0.97(10)	0.16(2)	0.16(2)
0.41	0.84(7)	0.08(1)	0.10(1)

as well [11, 16]. The ratios m_{orb}/m_{spin} of 0.10 to 0.16 are larger than the ones reported in the literature (0.030, 0.042 and 0.056 in [11, 15, 16]), a consequence of the slightly larger orbital and smaller spin magnetic moments we observed.

The size of the XMCD with respect to the XAS signal (see figure 1) and, consequently, the values for m_{spin} are much smaller than expected for a high-spin state but larger than for the low-spin state (a comparison to hysteresis measurements can be found in section S2 of the supplemental materials [40]). It appears that the samples are not fully saturated at the maximum applied field of 6 T, which should be the case for a fully ferromagnetic material. Instead, the two Fe sites could be ferrimagnetically ordered, resulting in a net magnetic moment with strong anisotropy. Another possibility is weak ferromagnetism resulting from ferrimagnetic order between Fe sites. These scenarios are more likely than the antiferromagnetic ground state theoretically predicted for the Fe_3GeTe_2 without Fe-deficiency [39], where strong exchange interactions dominate and much larger fields than 6 T would be needed for observing a canting of the spins.

3.2. Magnetic susceptibility

The ordering temperature can, in principle, be obtained from temperature-dependent XMCD measurements. However due to temperature stability and time constraints, it was more practical to probe the temperature dependence of the inverse dc magnetic susceptibility $1/\chi$ and its derivative $\mathrm{d}(1/\chi)/\mathrm{d}T$ for all crystals (see figure 2(a) and inset therein). The expression for the susceptibility stems from the spherical approximation where the magnetic levels are assumed to be equally spaced. This is certainly not the case for Fe^{2+} where the chemical bond dominates (crystal field and covalence). Therefore, relating the effective magnetic moment as determined by the susceptibility slope to the spin and orbital magnetic moments of the lowest lying level of Fe^{2+} is not straightforward and only an approximation.

All samples were field-cooled in a 100 Oe external magnetic field applied parallel to the *c*-axis. The common FC value of 100 Oe was chosen as it makes this study consistent with our previously reported work [38]. Furthermore, 100 Oe is a good compromise in terms of sensitivity, uniformity of the aligned moments, and avoidance of saturation. The sharp increase of χ is consistent with Curie's law $1/\chi = (T - T_C)/C$ for ferromagnetic materials from which the transition temperature T_C can be readily obtained. It is found to decrease from 205 to 138 K when the Fe deficiency increases from $\delta = 0.16$ to 0.41 (see figure 2(b)). The decrease of T_C is due to disorder and magnetic dilution introduced by the Fe deficiency [38]. This is best seen in the reduction of the spin and orbital magnetic moment from 1.26 to 0.84 μ_B/Fe and from 0.15 to 0.08 μ_B/Fe, respectively (see table 1).

The Curie constant C in the small field approximation is given as $C = \mu_0 n m_{eff}^2/3k_B$ with $m_{eff} = g\mu_B\sqrt{J(J+1)}$ the effective magnetic moment, n the electron density, and μ_0 and k_B the vacuum permeability and Boltzmann constant, respectively, g is the g-factor, μ_B the Bohr magneton, and J the total angular momentum quantum number [46]. The effective magnetic moment in this context has the dimension of a 'magnetic moment' but it is not a real magnetic moment in the sense that it is not an averaged value of an angular momentum. Assuming that the electron density is approximately the same in all samples, the Curie constant should be proportional to the effective magnetic moment, $C \propto m_{eff}$. Although both m_{eff} and C decrease with increasing Fe deficiency δ (see figure 2(c)), C falls off more sharply than m_{eff}. This indicates that the electron density n is varying between the samples—a consequence of the different Fe deficiencies and associated defect concentrations.

The Fe deficiency has been reported to induce a phase transition from an antiferromagnetic ground state to the ferromagnetic state often observed in experiments [39]. The fact that doping can instil the same magnetic phase transition and that gating can increase the Curie temperature T_c to room temperature points to a strong interdependence between magnetic and electronic properties—a consequence of Coulomb repulsions coupled to the Pauli exclusion principle. Furthermore, the Curie temperature T_c, magnetic anisotropy, and effective magnetization m_{eff} correlate directly with the Fe deficiency and decrease when the Fe deficiency decreases [10]. The stronger fall-off of the Curie constant C with increasing Fe deficiency δ can thus be explained by the two-fold dependency on the electron density, $C \propto n \cdot m_{eff}(n)$. Indications for a secondary transition at lower temperatures, which could indicate an antiferromagnetic phase, were not observed [47]. More susceptibility and hysteresis measurements at different temperatures can be found in section S3 of the supplemental materials [40].

3.3. Multiplet calculations

For a better understanding of the deficiency-dependent modifications of the XAS and XMCD spectra, crystal field multiplet calculations were performed using CRISPY [48]. To the best of our knowledge, this is the first attempt of reproducing the x-ray spectra of Fe_3GeTe_2 using such calculations, owing to the complexity of the different site symmetries and vacancy states. The best fit was obtained by a superposition of Fe^{2+} in dihedral symmetry (D_{3h}) and Fe^{3+} in octahedral symmetry (O_h) (see figure 3). Unfortunately, we cannot straightforwardly disentangle the contributions from the non-equivalent Fe I and Fe II sites to the Fe^{2+} and Fe^{3+} peaks because they overlap in the multiplet structure. The spectra were calculated for the *k* vector (propagation vector of the x-rays) pointing in the *z*-direction, i.e., parallel to the *c*-direction of the crystal. The calculations

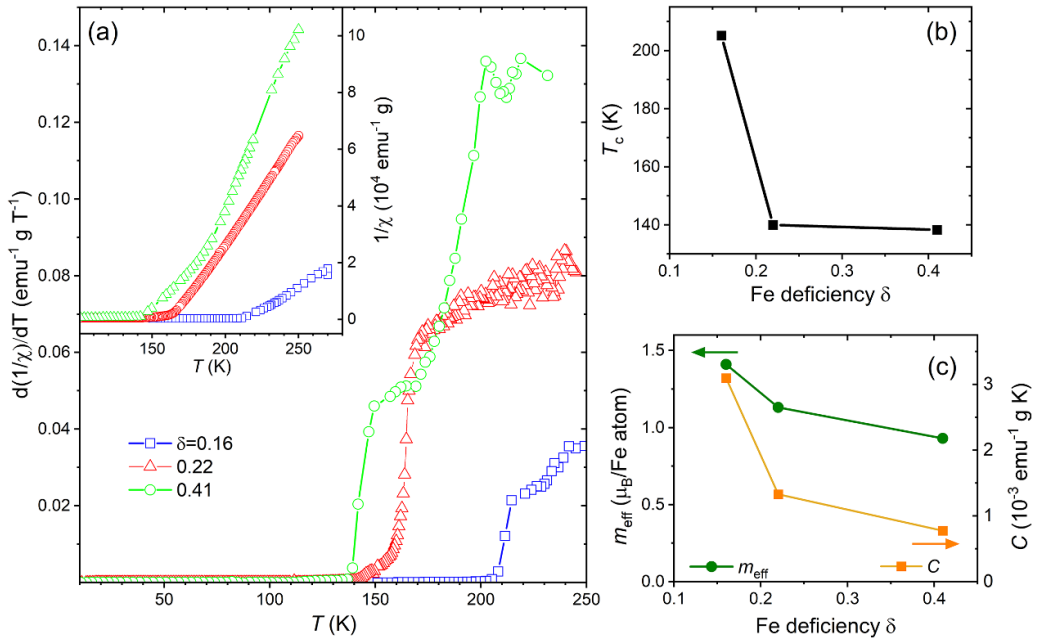

Figure 2. (a) Temperature dependence of the derivative of the inverse dc magnetic susceptibility $1/\chi$ for Fe deficiencies of $\delta = 0.16$ (blue squares), 0.22 (red circles), and 0.41 (green triangles). A field of 100 Oe was applied in the *c*-axis direction. The inset shows the inverse magnetic susceptibility $1/\chi$ as a function of the temperature. The Curie constant C can be obtained from the slope of this temperature dependence. (b) Dependence of the Curie temperature T_C on δ. (c) Dependence of m_{eff} and Curie constant C on δ. The errors in (b) and (c) are smaller than the symbols representing the data points.

were performed for an isotropic average with a Lorentzian FWHM broadening of 0.36 eV and Gaussian broadening of 1.5 eV. The sample with $\delta = 0.16$ was best fitted taking into account only the contribution of the Fe^{2+} state, i.e., the contribution from the Fe^{3+} state was negligible. The Fe^{3+} spectrum had to be shifted by 1.9 eV toward higher energies relative to the Fe^{2+} spectrum. The larger energy of the higher valence state is due to the larger Coulomb energy between the core hole and the *d* electron [49]. The fit parameters of the Slater integrals can be found in table 2. The values of the Slater integrals F and G, determining the size of the electron-electron repulsion and intra-atomic screening, respectively, were reduced to 80%. This ensures an accurate peak position for both the L_2 and L_3 peaks. For D_{3h} symmetry, the energy of the orbitals and the ligand field parameters can be found in the literature [50].

A perfect fit of the multiplet calculation to the experimental data is difficult to achieve. The reason is that multiplet calculations only take the main interactions into account, such as Coulomb and exchange, spin-orbit, crystal field and Zeeman interaction. They do not account for band structure effects, long-range order interactions, lower symmetry distortions and ligand field effects [44, 51, 52].

As can be seen in figure 3 the shape of the L_3 peaks could be reproduced, i.e. a single peak for a δ of 0.16 and double peaks for 0.22 and 0.41. However, while the shape of the L_2 peaks could be reproduced as well, the peak height was persistently larger, in particular at lower Fe content. The discrepancy could be slightly reduced by allowing charge transfer to Fe^{3+}, reducing its amplitude. Nevertheless, the physical justification for including charge transfer due to configuration interaction in our calculations remains unclear. There might be a different reason for the suppressed peak height which can be captured by including charge transfer between Fe^{2+} and Fe^{3+} configurations (but not sites). More theoretical investigations are clearly needed to shed light on this issue.

Since the measurements were taken in an applied magnetic field of 6 T using circularly polarized light, the multiplet calculations were compared to the mean of the spectra taken with pc and nc x-rays. The experimental and calculated XMCD spectra are shown in figure 3. Here, the agreement is somewhat better compared to the XAS spectra, with both L_2 and L_3 peaks exhibiting the correct height. The largest discrepancy is to the small positive L_3 peak, originating from the Fe^{3+} contribution, not found for the experimental spectra. While the mixing between the Fe^{2+} and Fe^{3+} XAS spectra was 7:3 for an Fe deficiency of 0.22, and 13:7 for 0.41 (the sample with Fe deficiency of 0.16 could only be fitted to Fe^{2+}), the ratio for the XMCD spectra was 9:1. Thus, the contribution of the Fe^{3+} state to the XMCD is far lower compared to its weight in the XAS spectra, hinting at a lower magnetic moment compared to the Fe^{2+} state.

To verify this observation, we carried out a sum rules analysis of the calculated spectra, both for the superposed and the two individual spectra. The results for the calculated spectra are shown in figure 4, where they can be compared to the sum rule results of the experimental spectra. We obtain good qualitative agreement between experiment and calculation, as the spin moment m_{spin} decreases with increasing Fe deficiency, while m_{spin} of the superposition underestimates the experimental values and is smaller than for the Fe^{2+} state alone. However, m_{spin} for the Fe^{3+} state is much smaller,

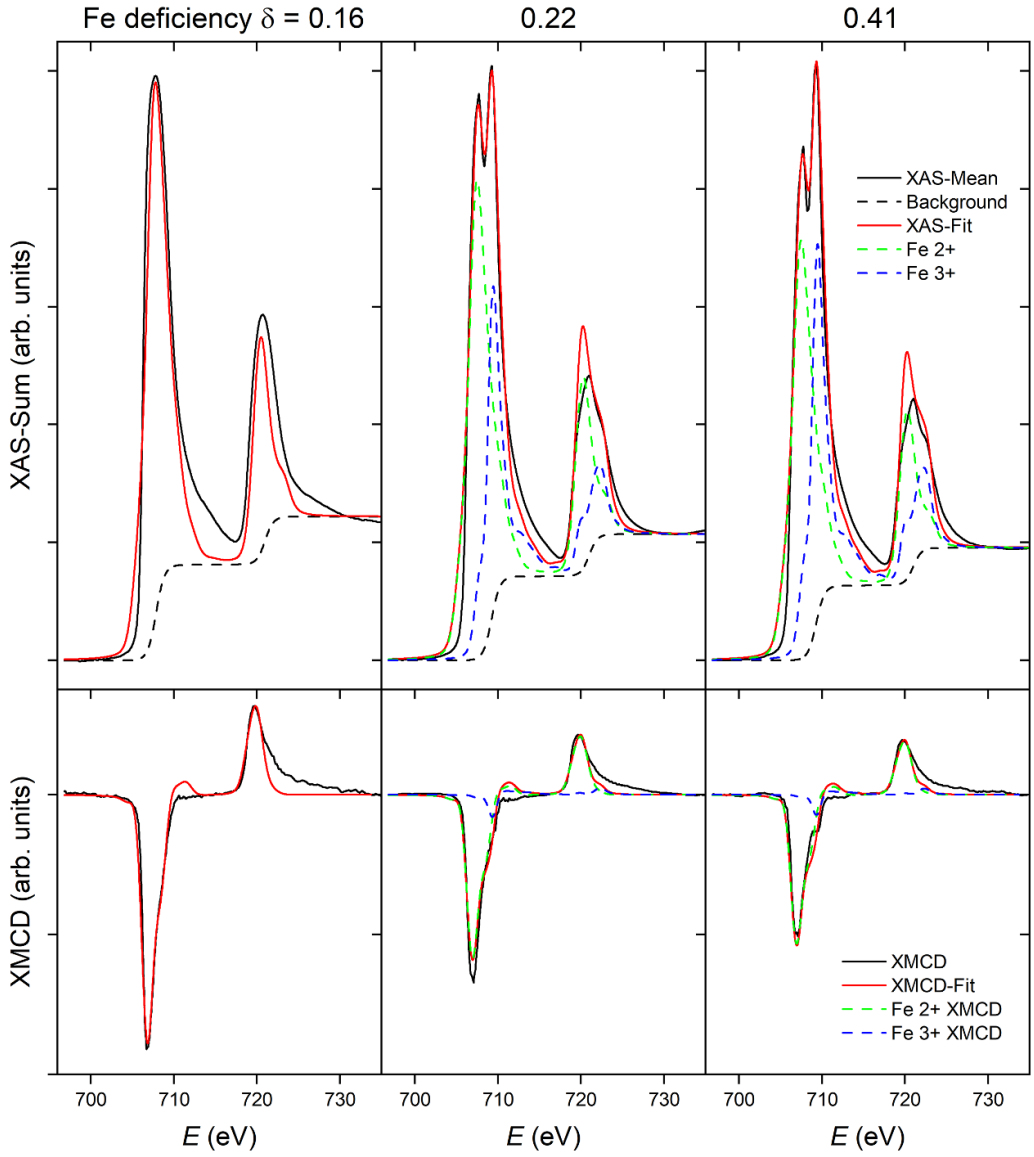

Figure 3. Experimental and calculated XAS and XMCD spectra for three different Fe contents. The fits (red lines) are superpositions of the calculated Fe^{2+} (green dashed lines) and Fe^{3+} (blue dashed lines) spectra.

Table 2. Parameters used for the XAS calculations for both Fe^{2+} and Fe^{3+} ions in units of eV. Parameters that cannot be determined for a given symmetry are indicated by a dash (—).

Ion	Symmetry	State	$F_{dd}^{(2)}$	$F_{dd}^{(4)}$	ζ_{3d}	$F_{pd}^{(2)}$	$G_{pd}^{(1)}$	$G_{pd}^{(3)}$	ζ_{2p}	$10Dq$	D_μ	D_σ
Fe^{3+}	O_h	Initial	9.634	6.028	0.053	—	—	—	—	1.0	—	—
		Final	10.255	6.419	0.067	5.957	4.451	2.532	8.200	1.0	—	—
Fe^{2+}	D_{3h}	Initial	8.773	5.452	0.052	—	—	—	—	—	0.13	−0.13
		Final	9.424	5.858	0.067	5.434	4.000	2.275	8.200	—	0.13	−0.13

resulting from the diminished weight of its XMCD compared to the XAS spectra. This of course affects the superposition as well.

The orbital magnetic moment m_{orb} exhibits a good agreement between superposition and experiment. The value for the Fe^{3+} state is very close to zero, because the integral q is close to zero. This orbital quenching effect is well-known for $3d$ ions, where crystal field effects are stronger than spin-orbit interaction—a direct consequence of the larger extension of those states away from the nucleus [53]. However, the Fe^{3+} state contributes significantly to the integral of the XAS spectra, leading to a smaller orbital moment of the superposition compared to the Fe^{2+} state alone. The orbital magnetic moment of the Fe^{2+} state is smaller than the calculated one due to the same quenching effect. However, it is not fully suppressed, as is the case for the Fe^{3+} state.

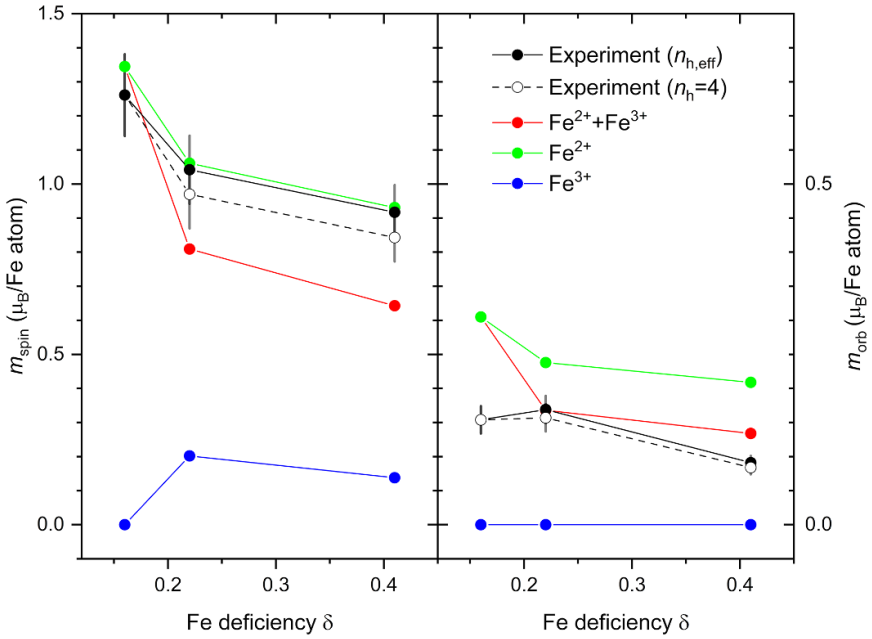

Figure 4. Summary of the m_{spin} and m_{orb} values obtained from the sum rules analysis of the experimental and calculated spectra. The calculated spectra for the Fe^{2+} and Fe^{3+} states have been analyzed both separately and as a superposition. The sum rules results from the experimental data are shown using $n_h = 4$ (black dashed line) and using an increased value $n_{h,eff}$ (black straight line).

We can only speculate about the origin of the Fe^{3+} state and its suppressed magnetic contribution. The upward shift in energy could indicate an oxidation effect. The higher charge of the Fe^{3+} compared to the Fe^{2+} state results in a stronger ligand field, in turn increasing the splitting between t_{2g} and e_g. This increases the likelihood of finding Fe^{3+} in a low-spin state, which indeed is observed in our experiment. Nevertheless, a $10D_q$ of 1 eV is too small to instigate a low-spin state. At least 2 eV would be needed for the crystal field to dominate the direct exchange interaction. Magnetic disorder, a signature of low magnetic moments, can be excluded since a 6 T magnetic field was applied, sufficient to saturate such a state. A possible explanation is anti- or ferrimagnetic ordering due to the nature of the exchange interaction. Under such circumstances, the magnetic field can be insufficient to align the moments.

Due to the mixture of the Fe^{2+} and Fe^{3+} states, a mixture of the hole number n_h can be assumed. Increased values of $n_h = 4.3$ and 4.35 were thus used in the sum rule analysis for the deficiencies $\delta = 0.22$ and 0.41, respectively. They were obtained using $n_{h,eff} = 4 \cdot w_{2+} + 5 \cdot w_{3+}$ where $w_{2+,3+}$ are the individual weights of the Fe^{2+} and Fe^{3+} contributions to the XAS. The number of *d*-holes for Fe^{2+} and Fe^{3+} were 4 and 5, respectively. This consideration ignores that the weight of the Fe^{3+} contribution to the XMCD is far smaller compared to the XAS. Hence, the increase of n_h might be an overestimation. Since no admixture with higher valence states was found in the $\delta = 0.16$ sample, the hole number was not modified and kept at a value of 4. The experimental results for $n_{h,eff}$ are shown as black straight line in figure 4 and for $n_h = 4$ as black dashed lines. The deficiency dependence of the spin moment stays largely the same when the effective hole numbers are used. The orbital moment is now clearly deficiency-dependent as well, underlining that the reduced Fe content affects both spin and orbital magnetic moments.

4. Conclusion

We have measured XAS and XMCD spectra of $Fe_{3-\delta}GeTe_2$ single crystals with varying Fe deficiencies, and performed multiplet calculations to reproduce the experimental spectra. A sum rules analysis of both the experimental and calculated spectra showed in both cases a clear reduction of the spin moment with increasing Fe deficiency. While the values of the orbital magnetic moments are smaller, this trend remains the same. Magnetic susceptibility measurements show that the reduction in magnetization is accompanied by a reduced Curie temperature. Moreover, the tendency for the Fe deficiency to vary within the same crystal explains why flakes from the same crystal can exhibit significantly different magnetic properties.

The multiplet calculations give insight into the origin of the XAS and XMCD spectra, composed of a Fe^{2+} state and, in case of increasing Fe deficiency, an additional Fe^{3+} state. While a stronger Fe deficiency reduces the spin and orbital magnetic moments in both experiment and calculation, the suppression of these moments in the Fe^{3+} state exacerbates the effect, as is evident in the lower values obtained in the superposed compared to the Fe^{2+} state only. A better quantitative agreement would necessitate a better agreement between the calculated and experimental spectra, which might be achieved by exploring a greater parameter space. However, the good qualitative agreement allowed us to better understand the electronic and magnetic structure of Fe-deficient Fe_3GeTe_2 single crystals. In particular, we demonstrate directly the correlation of Fe deficiency, appearance of an additional Fe^{3+}

state, and reduced magnetic moment. Such variations of the magnetic moment can occur between pieces of the same crystal which are then fully characterized.

A detailed understanding of the effect beyond multiplet calculations is difficult as it involves fully understanding the defect chemistry in Fe_3GeTe_2, which has not been accomplished yet. Our work demonstrates the adverse impact of small deviations of the Fe stoichiometry on the magnetic properties. This has direct implications for the assembly of high-quality 2D magnet systems, exfoliated from such Fe_3GeTe_2 single crystals. Our work thus contributes directly to any future endeavor to integrate 2D magnets in spintronic devices with improved or novel capabilities.

Data availability statement

All data that support the findings of this study are included within the article (and any supplementary files).

Acknowledgments

Work at the University of Warwick was supported by EPSRC, UK through Grants EP/N032128/1 and EP/T005963/1. Diamond Light Source is acknowledged for the provision of beamtime on beamline I06 under proposal MM27482. We acknowledge Diamond Light Source for providing access to the SQUID magnetometer in their Materials Characterisation Laboratory.

ORCID iDs

D Backes https://orcid.org/0000-0002-1019-3323
G D A Wood https://orcid.org/0000-0002-3709-5213
G Balakrishnan https://orcid.org/0000-0002-5890-1149
G van der Laan https://orcid.org/0000-0001-6852-2495
T Hesjedal https://orcid.org/0000-0001-7947-3692

References

[1] Novoselov K S, Geim A K, Morozov S V, Jiang D, Zhang Y, Dubonos S V, Grigorieva I V and Firsov A A 2004 *Science* **306** 666
[2] Mermin N D and Wagner H 1966 *Phys. Rev. Lett.* **17** 1133
[3] Huang B *et al* 2017 *Nature* **546** 270
[4] Gong C *et al* 2017 *Nature* **546** 265
[5] Fei Z *et al* 2018 *Nat. Mater.* **17** 778
[6] Deiseroth H J, Aleksandrov K, Reiner C, Kienle L and Kremer R K 2006 *Eur. J. Inorg. Chem.* **2006** 1561
[7] Chen B, Yang J, Wang H, Imai M, Ohta H, Michioka C, Yoshimura K and Fang M 2013 *J. Phys. Soc. Jpn.* **82** 124711
[8] Li Q *et al* 2018 *Nano Lett.* **18** 5974
[9] Kong X, Nguyen G D, Lee J, Lee C, Calder S, May A F, Gai Z, Li A P, Liang L and Berlijn T 2020 *Phys. Rev. Mater.* **4** 094403
[10] May A F, Calder S, Cantoni C, Cao H and McGuire M A 2016 *Phys. Rev.* B **93** 014411
[11] Zhu J X *et al* 2016 *Phys. Rev.* B **93** 144404
[12] Tian C K, Wang C, Ji W, Wang J C, Xia T L, Wang L, Liu J J, Zhang H X and Cheng P 2019 *Phys. Rev.* B **99** 184428
[13] Hwang I, Coak M J, Lee N, Ko D S, Oh Y, Jeon I, Son S, Zhang K, Kim J and Park J G 2019 *J. Phys.: Condens. Matter* **31** 50LT01
[14] Liu B *et al* 2020 *Phys. Rev. Lett.* **125** 267205
[15] Lopes J M J *et al* 2021 *2D Mater.* **8** 041001
[16] Yamagami K *et al* 2021 *Phys. Rev.* B **103** L060403
[17] Ding S *et al* 2021 *Phys. Rev.* B **103** 094429
[18] Zhang Y *et al* 2021 *Appl. Phys. Lett.* **118** 262406
[19] Fujimura R, Yoshimi R, Mogi M, Tsukazaki A, Kawamura M, Takahashi K S, Kawasaki M and Tokura Y 2021 *Appl. Phys. Lett.* **119** 032402
[20] Wu X *et al* 2021 *Phys. Rev.* B **104** 165101
[21] Gao Y *et al* 2022 *Phys. Rev.* B **105** 014426
[22] Bao S *et al* 2022 *Phys. Rev.* X **12** 011022
[23] Huang X, Xu J, Nie X, Chen C, Wang W, Song G, Jiang X and Liu J M 2022 *Appl. Phys. Lett.* **120** 073106
[24] Kim K *et al* 2018 *Nat. Mater.* **17** 794
[25] You Y *et al* 2019 *Phys. Rev.* B **100** 134441
[26] Zhang Y *et al* 2018 *Sci. Adv.* **4** eaao6791
[27] Zhuang H L, Kent P R C and Hennig R G 2016 *Phys. Rev.* B **93** 134407
[28] Deng Y *et al* 2018 *Nature* **563** 94
[29] Dzyaloshinsky I A 1958 *J. Phys. Chem. Solids* **4** 241
[30] Nguyen G D, Lee J, Berlijn T, Zou Q, Hus S M, Park J, Gai Z, Lee C and Li A P 2018 *Phys. Rev.* B **97** 014425
[31] Ding B, Li Z, Xu G, Li H, Hou Z, Liu E, Xi X, Xu F, Yao Y and Wang W 2020 *Nano Lett.* **20** 868
[32] Chowdhury R R, DuttaGupta S, Patra C, Sharma S, Fukami S, Ohno H and Singh R P 2021 *Sci. Rep.* **11** 14121
[33] Park T E *et al* 2021 *Phys. Rev.* B **103** 104410
[34] Peng L, Yasin F S, Park T E, Kim S J, Zhang X, Nagai T, Kimoto K, Woo S and Yu X 2021 *Adv. Funct. Mater.* **31** 2103583
[35] Wu Y *et al* 2022 *Adv. Mater.* **34** 2110583
[36] Corasaniti M, Yang R, Sen K, Willa K, Merz M, Haghighirad A A, Tacon M L and Degiorgi L 2020 *Phys. Rev.* B **102** 161109(R)
[37] Watson M D *et al* 2013 *New J. Phys.* **15** 103016
[38] Mayoh D A, Wood G D A, Holt S J R, Beckett G, Dekker E J L, Lees M R and Balakrishnan G 2021 *Cryst. Growth Des.* **21** 6786
[39] Jang S W, Yoon H, Jeong M Y, Ryee S, Kimb H S and Han M J 2020 *Nanoscale* **12** 13501
[40] Supplementary information
[41] Thole B T, Carra P, Sette F and van der Laan G 1992 *Phys. Rev. Lett.* **68** 1943
[42] Carra P, Thole B T, Altarelli M and Wang X 1993 *Phys. Rev. Lett.* **70** 694
[43] Chen C T, Idzerda Y U, Lin H-J, Smith N V, Meigs G, Chaban E, Ho G H, Pellegrin E and Sette F 1995 *Phys. Rev. Lett.* **75** 152
[44] van der Laan G and Figueroa A 2014 *Coor. Chem. Rev.* **227** 95
[45] Piamonteze C, Miedema P and de Groot F M F 2009 *Phys. Rev.* B **80** 184410
[46] Coey J M D 2009 *Magnetism and Magnetic Materials* (Cambridge University Press)
[47] Yi J, Zhuang H, Zou Q, Wu Z, Cao G, Tang S, Calder S A, Kent P R C, Mandrus D and Gai Z 2017 *2D Mater.* **4** 011005
[48] Retegan M 2019 Crispy: v0.7.3 (available at: https://dx.doi.org/10.5281/zenodo.1008184)
[49] van der Laan G and Kirkman I W 1992 *J. Phys.: Condens. Matter* **4** 4189–204
[50] Konig E and Kremer S 1977 *Ligand Field Energy Diagrams* (Plenum Press)
[51] van der Laan G 2006 *Lect. Notes Phys.* **697** 143
[52] de Groot F M F *et al* 2021 *J. Electron Spectrosc. Relat. Phenom.* **249** 147061
[53] Blundell S 2001 *Magnetism in Condensed Matter* (Oxford University Press)